A Coupled Hydrodynamic–Bottom Boundary Layer Model of Storm and Tidal Flow in the Middle Atlantic Bight of North America*

TIMOTHY R. KEEN** AND SCOTT M. GLENN

Institute of Marine and Coastal Sciences, Rutgers University, New Brunswick, New Jersey

(Manuscript received 12 October 1993, in final form 1 August 1994)

ABSTRACT

The effects of increased friction and tides on circulation in the Middle Atlantic Bight (MAB) during the SWADE storm of 25–28 October 1990 have been investigated using a three-dimensional hydrodynamic model coupled to a bottom boundary layer model that calculates combined wave–current bottom drag coefficients. Winds were initially parallel to the coast (downwelling favorable) throughout the MAB, first shifting to offshore within the central MAB and then in the northern MAB, while remaining parallel to the coast within the southern MAB. The wind-driven circulation was approximately alongshore, with an onshore component at the surface and an offshore component at depth associated with downwelling. Compared to model runs with a pure current bottom friction formulation, the additional bottom friction in the coupled model decreased currents uniformly in shallow water and caused slight offshore rotation during downwelling circulation, but the effects were limited because of the persistent stratification and the variable wind field during the storm. The effect of tides was much more pronounced, since across-shelf tidal currents were of similar or greater magnitude than the wind-driven currents. The combination of downwelling offshore flow and tidal flow during the storm resulted in weaker bottom currents directed nearly alongshore during flood and stronger currents directed nearly offshore during ebb. Bottom shear stresses were initially highest when storm currents were largest and again later during ebb tides when tidal and storm bottom flows were in the same direction. These results suggest that sedimentation during the storm was directly related to the tidal flow.

1. Introduction

The storm current regime within the Middle Atlantic Bight (MAB) has been described by Swift et al. (1986) as consisting of a high frequency (6–12 s) wave orbital component superimposed on three-layer Ekman flow; stratified flow and coastal jets caused by freshwater runoff; steady alongshelf flow maintained by potential vorticity and geostrophy; relaxation currents associated with topographically trapped waves; and storm-surge ebb flows. The resulting bottom currents attain speeds of the order of 20 cm s^{-1} depending on water depth (e.g., Scott and Csanady 1976; Butman et al. 1979; Lyne et al. 1990a). The response of the MAB to a storm with an offshore path is characterized by coastal water levels rising first in the south as the storm approaches and throughout the MAB as the storm center passes to the northeast (Beardsley and Haidvogel 1981). The spinup time for the response is approximately 12 hours. This interval is short compared to the 2–10-day time scales of storm forcing, and the storm flow can therefore be treated as quasi steady. Beardsley and Haidvogel (1981) identified transient oscillations associated with local friction, inertial responses, and the adjustment of the entire region to impulsive forcing. The most energetic response has a period of approximately 6 hours and is damped within 1–2 days in shallow water by bottom friction.

Tidal flow is superimposed on storm circulation and introduces periodic variations in sea surface height and currents at diurnal and semidiurnal frequencies. Tidal amplitudes along the MAB coast are approximately 50 cm, and mean currents on the inner shelf are of the order of 10–20 cm s^{-1} (Blumberg and Kantha 1985). It appears reasonable, therefore, to consider tidal currents as an important unsteady component of storm flow. Blumberg and Kantha (1985) investigated the response of the MAB to a winter storm with an offshore storm track using a three-dimensional model that included the semidiurnal M_2 tidal component. Because they used climatological mean transports at the cross-shelf boundaries, their results revealed uniform southwestward flow at the surface with maximum currents within the central part of the MAB. They did not discuss interactions between tidal and storm currents, however.

---

* Contribution Number 94-23 of the Institute of Marine and Coastal Sciences, Rutgers University.

** Current affiliation: Naval Research Laboratory, Stennis Space Center, Mississippi.

Corresponding author address: Dr. Timothy R. Keen, Naval Research Laboratory, Code 7320, Stennis Space Center, MS 39529.

The motivation for the present study is to examine the fluid processes that govern sediment resuspension and transport during storms on the MAB continental margin. For example, the general sedimentation regime for the MAB can be characterized as accommodation dominated (Swift and Thorne 1991), with sedimentation governed by fluid motion instead of sediment input from the coast. Measurements of bottom currents and sediment concentrations within the MAB reveal regional transport to the southwest at timescales of months to years (Butman et al. 1979; Vincent et al. 1981). However, the importance of storms in transporting sediment at shorter timescales has been documented for both the inner and outer shelves (e.g., Gadd et al. 1978; Lyne et al. 1990a,b). These studies were unable to correlate observations at separated stations because of the unknown effects of advection. Thus, it is necessary to use models of sedimentation in conjunction with observations to understand sedimentation at the event scale, that is, hours to days.

Deterministic numerical approaches have been slow to develop because of the difficulty in coupling circulation and sediment transport models. Spaulding and Isaji (1987) successfully incorporated a simplified version of the Grant and Madsen (1979) bottom boundary layer model (BBLM) into a three-dimensional hydrodynamic model of circulation during Tropical Storm Delia and demonstrated the importance of combined wave–current stresses on storm flows. They also evaluated both model and field results using the suspended sediment stratification model of Glenn and Grant (1987) and demonstrated the importance of suspended sediment on bottom stresses. More recently, Davies and Lawrence (1993) used a similar approach to evaluate the interaction of tidal and wind-driven currents and noted the importance of tidal currents in producing maximum bed stresses. Keen and Slingerland (1993a,b) evaluated sedimentation during tropical cyclones with a combined circulation–sedimentation model. They identified several atmospheric and physiographic controls on storm sedimentation. However, because of the small tides and generally well-mixed conditions during hurricanes in the Gulf of Mexico, they neglected tidal forcing and stratification. Tides are greater within the MAB, and stratification may persist over a large region affected by the storm, depending on the amount and duration of mixing. Recent work has demonstrated the role of stratification and bed friction in determining bottom flow on stratified continental shelves (Keen and Glenn 1994). These considerations require the inclusion of both tides and stratification if sedimentation is to be evaluated using numerical models of storm-dominated, midlatitude shelves like the MAB.

This paper evaluates bottom friction and storm flow on a stratified continental shelf where tidal and storm bottom currents can be of similar magnitude. Using the coupled model described by Keen and Glenn (1994), this problem is addressed by hindcasting circulation during a northeaster storm that passed over the MAB during Intense Observation Period IOP-1 (20–31 Oct 1990) of the Surface Wave Dynamics Experiment (SWADE) (Weller et al 1991; Caruso et al. 1993). The effects of increased bottom friction without tidal forcing are investigated in several experiments that used both small and large values of a spatially and temporally constant bottom roughness parameter k_b. Variable bottom friction is introduced using the coupled model, which calculates combined wave–current bottom drag coefficients. The evolution of combined tidal and storm-driven flow is then evaluated using the wave–current bottom friction model. Finally, the hindcast results are discussed in terms of implications for shelf circulation and sediment transport during storms within the MAB.

2. The Middle Atlantic Bight model

Stratification of the water column is expected to persist over large parts of the shelf within the MAB during extratropical cyclones, and for this reason it is important to include turbulent mixing of mass, momentum, and heat in calculating the coastal flow field. Thus, the turbulent energy hydrodynamic model described by Keen and Slingerland (1993a) is used to calculate the evolution of the sea surface height, circulation, salinity, temperature, and turbulent kinetic energy fields in this study. For a description of the turbulent energy closure scheme applied in the model, the reader is referred to Leendertse and Liu (1977) and Keen and Slingerland (1993a). The turbulent energy algorithm calculates turbulent vertical mixing while allowing extreme wind forcing and realistic density stratification. Horizontal subgrid-scale mixing is found from the curl of the velocity field, with a minimum value of 10^8 cm^2 s^{-1} for the eddy diffusivity used in this study to improve the tidal response when compared to coastal observations. This model has been extensively evaluated for tidal flows in estuaries and coastal seas (e.g., Liu and Leendertse 1978), as well as hurricane flows in the Gulf of Mexico (Keen and Slingerland 1993b).

The hydrodynamic equations are solved on an Arakawa C grid in a Cartesian coordinate system at a fixed latitude of 39°N (the f-plane approximation). The model grid is aligned with the y axis parallel to the coast within the central MAB (Fig. 1). Model grid points are evenly spaced at 15 km along both horizontal axes. There are 33 grid points along the x axis and 67 along the y axis. The z axis is represented by eight levels with constant thickness throughout the model grid: levels 1–3 are each 10 m thick, 4–6 are each 20 m thick, level 7 is 110 m thick, and level 8 is 200 m thick. This choice of level thicknesses results in 10-m bottom levels on the inner shelf (water depths less than 30 m) and 20-m bottom levels on the outer shelf (water depths from 50 to 90 m). Although the water column

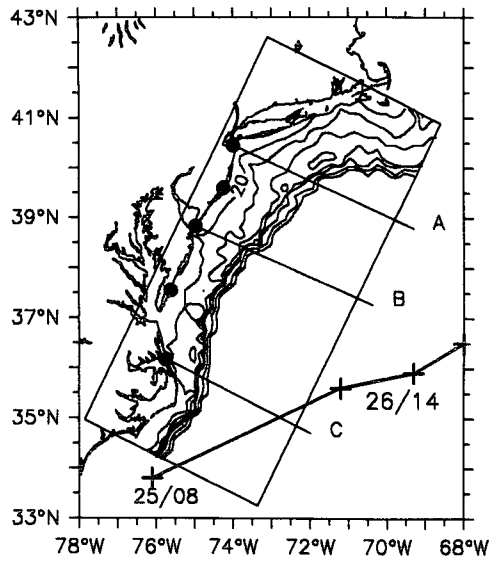

FIG. 1. Outline of the MAB model grid on the regional map with model bathymetry contoured at intervals of 20, 30, 50, 70, 90, 200, and 400 m, coinciding with the bottom of model levels. Cross sections A, B, and C are discussed in the text. Coastal tidal stations (indicated by the solid circles) referred to in the text are, from north to south: Sandy Hook, Atlantic City, and Cape May, New Jersey; Wachapreague Island, Virginia; and Duck Pier, North Carolina. The position of the storm low pressure center at 0800 EDT 25 Oct, and 0800 and 1400 EDT 26 Oct is indicated by crosses.

is not resolved in detail by this choice of levels, similar level thicknesses were sufficient to reproduce reasonably well the measured currents near the surface and bed during Tropical Storm Delia (Keen and Slingerland 1993a).

To calculate the time-averaged combined wave and current shear stresses within the bottom boundary layer, the coupled hydrodynamic–bottom boundary layer model described by Keen and Glenn (1994) has been developed. The eddy viscosity profile within the bottom boundary layer is represented by inserting the BBLM within the lowermost hydrodynamic model level. This formulation also increases the vertical resolution of currents within the bottom boundary layer. Keen and Glenn (1994) discuss model results for stratified flow in coastal water depths using the coupled model with 5-m level thicknesses. An evaluation of their results shows that the vertical current structure does not significantly change over a depth range of 10–20 m near the bottom. Thus, using a level 20 m thick to represent the lowermost water column on the outer shelf should not significantly affect the calculated flow field. The present study focuses on storm flow in depths of 90 m or less on the continental shelf; therefore, the vertical resolution of the model is reduced seaward of the 90-m isobath, and the continental slope and deep sea are represented by a flat bottom 400 m in depth. This shallow depth is used to allow larger time steps in integrating the model equations. Previous work has shown that it does not significantly alter the calculated storm flow on the shelf (Keen and Slingerland 1993a,b). Initial stratification was taken as mean October salinity and temperature profiles for the New York Bight (Bowman 1977).

No flow is permitted perpendicular to the landward boundary or the cross-shelf boundaries at $y = 2$ (southwest) and $y = 65$ (northeast). A closed cross-shelf boundary condition is used because it avoids the instabilities that occurred with other boundary conditions because of the variable wind stresses and tidal forcing at the open seaward boundary. Although end effects are present in the model results, the boundaries have been placed so as to limit their interference with flows calculated during the hindcast interval for the continental shelf from New York Harbor to Cape Hatteras. The most significant end effect was in the northeast corner, where surface water levels were 10 cm below MSL during the storm peak. This resulted in diminished alongshelf pressure gradients and flow speeds throughout the northeastern part of the MAB but outside of our study area. Flow within the MAB was unperturbed by the closed boundary in the south because of the projection of Cape Hatteras.

When tidal forcing was included, the water surface height at the seaward boundary was calculated using M_2 and K_1 components of 20 and 4 cm, respectively (Schwiderski 1979; Neumann and Pierson 1966). No north–south phase difference was used in computing tidal forcing because the tidal wave reached the northern landward boundary first, resulting in a phase difference of the proper sign and magnitude. Transport of momentum, mass, heat, and turbulent energy across the open boundary is treated using an admittance condition. On inflow, the initial values of salinity and temperature are introduced at the open boundary, whereas during outflow the values calculated by the model are used. Horizontal currents also vary over a tidal cycle, with the restriction that no net transport out of the model grid can occur. The combination of closed cross-shelf boundaries and the periodic seaward boundary conserves mass within the model domain. When tidal forcing is neglected, the seaward boundary is closed.

An additional source of flow within the MAB model grid is the Gulf Stream. Observations within the MAB indicate that Gulf Stream frontal eddies can influence circulation and water properties on the shelf (Glenn and Ebbesmeyer 1994), but because these are intermittent and primarily limited to the region immediately north of Cape Hatteras, the present study neglects this flow. The model domain has been extended south of Cape Hatteras to avoid end effects within the MAB.

The coupled model calculates bottom friction using a quadratic drag coefficient that can be constant or computed by a version of the wave–current interaction model of Grant and Madsen (1979) that has been modified and extended to cover a wider range of conditions with increased efficiency (Keen and Glenn

1994). The wave–current bottom drag coefficients are found using wave and current parameters for each grid point at each time step. The required input to the BBLM is the steady current u_r at a reference height z_r, the oscillatory bottom current u_b and excursion amplitude A_b, the angle between the current and wave $\bar{\varphi}_c$, and the physical bottom roughness k_b. Since there is very little vertical variation in the current profiles away from the bed, the reference height z_r was set to a constant of 2.5 m as in the study of Keen and Glenn (1994). This assumption standardized the bottom boundary layer calculations. The BBLM was only used to calculate the combined wave–current bottom stresses for model depths of 90 m or less. Since the spectral peak periods during the storm only reached a maximum of about 12 s, bottom wave-induced flows were not experienced at water depths of 200 and 400 m, and the pure current bottom stress was calculated at these grid points.

The hindcasts used a time step of 60 s for the 84-h storm duration. Prior to the storm, the model was run for 21.56 hours of simulation time with tidal forcing only. This procedure initialized sea surface heights to match the observed coastal water levels at 2000 EDT 24 October when the hindcasts began.

3. The SWADE storm

Three separate storm systems passed over the MAB during IOP-1. The SWADE storm was the middle storm and the most severe. It developed as a low off the North Carolina coast on 24 October (Caruso et al. 1993). Hourly hindcast fields of significant wave height H_S, peak wave period, mean wave travel direction (H. C. Graber, personal communication 1992), and wind speed and direction (V. Cardone, personal communication 1992) were supplied for the SWADE storm. These fields, bounded by 35°N on the south and 70°W on the east, were extrapolated to the edges of the model grid (see Fig. 1). The wave orbital parameters at the sea floor were found every hour using linear wave theory. The wind stress at each grid point was updated hourly from the hindcast wind speeds using drag coefficients that depend on the wind speed, wave period, and local water depth (Johnson and Vested 1992).

The hindcast storm winds were uniformly from the northeast at 2200 EDT 25 October (Fig. 2a), and the calculated surface stresses exceeded 3 dyn cm^{-2} in the southern MAB. Because of the southerly winds, both H_S and peak wave periods (not shown) increased southward. The wind stresses increased to more than 4 dyn cm^{-2} at 0745 EDT 26 October (Fig. 2b), by which time the wind had rotated anticlockwise in the south to become parallel to the coast. The storm wave field continued to strengthen southward. By 1730 EDT (Fig. 2c) the storm had moved seaward and the winds were turning offshore over much of the MAB. The wind stresses continued to weaken as the storm center passed into the North Atlantic, and at 0315 EDT 27 October (Fig. 2d) the wind stresses over the MAB were generally less than 2 dyn cm^{-2}. Despite a weakening of the winds, H_S remained above 3 m on the shelf.

4. The effects of increased bottom roughness without tides

Three hindcasts, MABS13, 14, and 16 (see Table 1), were used to examine the effects of increased bottom roughness on coastal circulation without tides. Hindcasts MABS13 and MABS14 used constant bottom drag coefficients C_d of 0.00127 and 0.00365, corresponding to bottom roughness heights k_b of 0.1 and 10 cm, respectively. Hindcast MABS16 used the BBLM to compute wave–current bottom drag coefficients, also assuming a bottom roughness k_b of 10 cm. The larger k_b approximates the increased bottom roughness associated with the ripple field and near-bed transport during a storm in shelf water depths. For example, ripple heights of 10–20 cm and lengths of 30–60 cm have been documented in water depths of 15–25 m on numerous video transects on the central New Jersey shelf. For this ripple geometry the Grant and Madsen (1982) bottom roughness model returns values of k_b on the order of 100 cm. During storms, however, ripples are expected to be partially washed out, reducing the ripple roughness. When this happens the bottom roughness will be dominated by near-bed transport, which can be an order of magnitude smaller than the ripple roughness. Therefore, a k_b value of 10 cm was chosen to approximate the expected movable bed roughness during high energy conditions.

Turbulent mixing in the coupled model occurs slowly for moderate wind stresses on an idealized straight coast (Keen and Glenn 1994), requiring about 48 hours to fully mix summer stratification profiles near shore. Downwelling breaks down stratification near the bed, however, because of seaward transport of less-dense water near the bottom, whereas upwelling reinforces stratification because of landward transport of cold bottom water from offshore (Trowbridge and Lentz 1991). Calculated wind stresses during the SWADE storm exceeded the value of 1.4 dyn cm^{-2} used in the test cases discussed by Keen and Glenn (1994) for less than 48 hours, and turbulent mixing was therefore limited. However, stratification was reduced on the outer shelf within the southern MAB because of consistently faster currents and larger waves than elsewhere. At a water depth of 70 m along section C (Fig. 3a, see Fig. 1 for location), mixing occurred at the base of the surface mixed layer in all three hindcasts although stratification near the surface decreased only slightly. Less mixing occurred at 90 m (Fig. 3b) because of a reduction in wave-induced turbulence in deeper water. Increased bottom friction had no discernible effect on mixing at 90 m. Stratification at 200 m was the

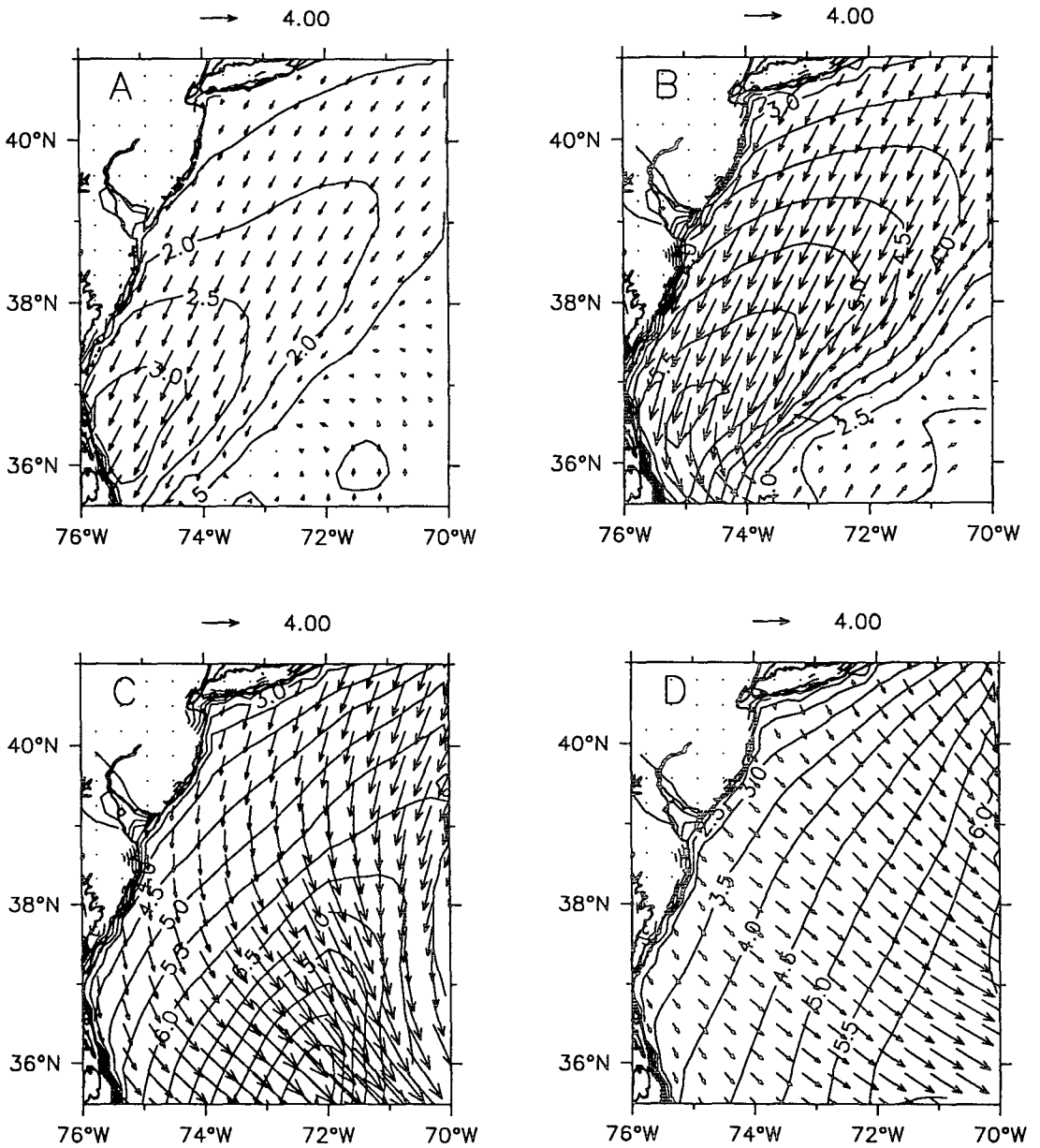

FIG. 2. Contour maps of hindcast significant wave heights in meters from the SWADE storm superimposed on wind stress vectors (dyn cm^{-2}) calculated from the hindcast SWADE winds at (a) 2200 EDT 25 Oct, (b) 0745 EDT 26 Oct, and (c) 1730 EDT and (d) 0315 EDT 27 Oct.

same in all three hindcasts because wave–current bottom stresses were not used at this water depth. These results suggest that stratification was not eliminated during the SWADE storm because of the moderate turbulent mixing on the shelf.

The storm winds were downwelling favorable over the central and southern MAB through the early afternoon of 26 October, and when tides were absent surface flow was to the south (Fig. 4). Currents increased southward with proximity to the storm track. Part of the reason for the weak flow in the north was the closed cross-shelf boundary, which prevented inflow at Cape Cod. For this reason, the hindcast results east of Long Island are not discussed here. Shelf circulation in the south was unaffected by the southern closed boundary because of the natural seaward deflection of the flow around Cape Hatteras. The uniform southerly winds over the central MAB along transect B (see Fig. 1 for location) transported surface water landward on the outer shelf (Fig. 5a), which drove downwelling flow by 1000 EDT 26 October in hindcast MABS13. Flow near the coast was primarily in the wind direction with

TABLE 1. Hindcast conditions.

Hindcast	k_b (cm)	C_d	Tidal amplitude (cm)
MABS13	0.1	0.00127	None
MABS14	10	0.00365	None
MABS15	0.1	BBLM[a]	None
MABS16	10	BBLM	None
MABS17	10	BBLM	$M_2 = 25$, $K_1 = 4$
MABS18	0.1	BBLM	$M_2 = 25$, $K_1 = 4$
MABS19	10	0.00365	$M_2 = 25$, $K_1 = 4$

[a] BBLM: C_d calculated by the bottom boundary layer model.

a very small offshore component that increased seaward at the bottom. The effect of computing C_d with the BBLM (run MABS16) can be seen in a cross section of the vector changes in cross-shelf flow between the low-drag and coupled model results (Fig. 5b). In water depths greater than 20 m, flow was deflected seaward throughout the water column because of increased bottom friction. Thus, weakly onshore flow at mid-depth on the outer shelf shifted to offshore, and downwelling flow at the shelf break increased. Near the coast, however, the response to increased bed drag was more complex. Surface and bottom currents were more collinear with the wind direction and current speeds were reduced by approximately 50% relative to hindcast MABS13. The differences in cross-shelf flow for a larger constant C_d (hindcast MABS14) were similar to those in Fig. 5b but the magnitudes were significantly smaller.

The storm winds along transect B at 2230 EDT 26 October were offshore, but cross-shelf transport was weak (Fig. 6a). Surface currents had a maximum offshore component of less than 5 cm s^{-1} in shallow water, and upwelling flow was weak on the outer shelf. The vector change in cross-shelf flow (Fig. 6b) when C_d was calculated by the BBLM reveals that currents were uniformly deflected landward near the coast while being rotated seaward in deeper water. The existence of downwelling currents at the shelf break suggests that upwelling was delayed by several hours relative to the low-drag case. The lag in the transition from downwelling to weak upwelling at section B occurred because greater bottom friction increased the response time of the coastal flow to changes in the wind direction. When a larger constant drag coefficient was used (hindcast MABS14), the magnitudes of the changes were half those seen in Fig. 6b, and weak upwelling was evident near the coast.

Time series of coastal water levels from hindcasts MABS14 and MABS16 (Fig. 7) lack the tidal signal recorded at the coastal stations. However, the timing of the hindcast storm surge does coincide with the general increase in observed water levels. Calculated coastal water levels were similar in both models until the storm peak, after which those from the coupled model (MABS16) were lower in the south, coinciding with

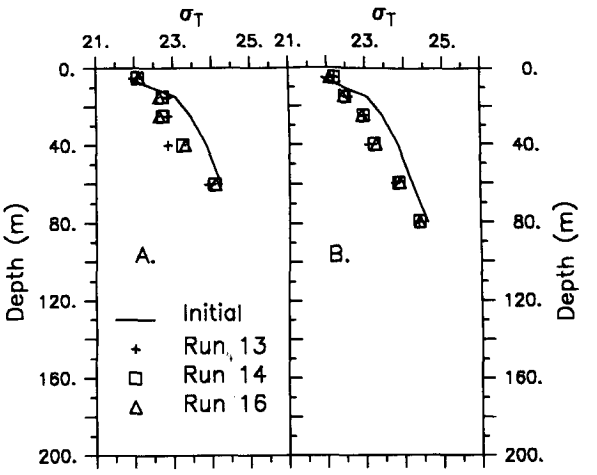

FIG. 3. Profiles of σ_T calculated for 0500 EDT 27 Oct at section C at water depths of (a) 70 m and (b) 90 m by the uncoupled model with constant drag coefficients of 0.00127 (+) and 0.00365 (□), and the coupled model with $k_b = 10$ cm (Δ). The initial profile is indicated with a solid line.

the southward increase in significant wave heights. As long as storm waves remained high on the shelf, bottom friction was greater in the coupled model, and bottom currents in shallow water were weaker than when a constant C_d was used. The combination of these reduced currents and a decrease in wave heights and periods as the storm winds turned offshore and weakened produced smaller bed stresses for several hours following the storm peak in MABS16, thus permitting larger storm-surge ebb currents for a short interval. Transient

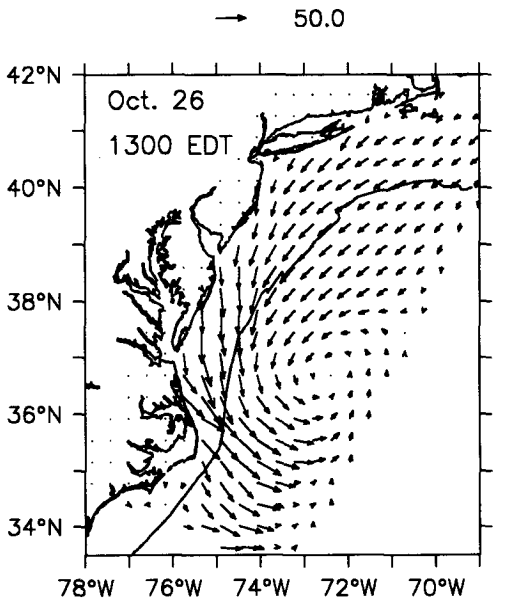

FIG. 4. Surface flow field for run MABS13 at 1300 EDT 26 Oct. The solid offshore line is the 200-m isobath.

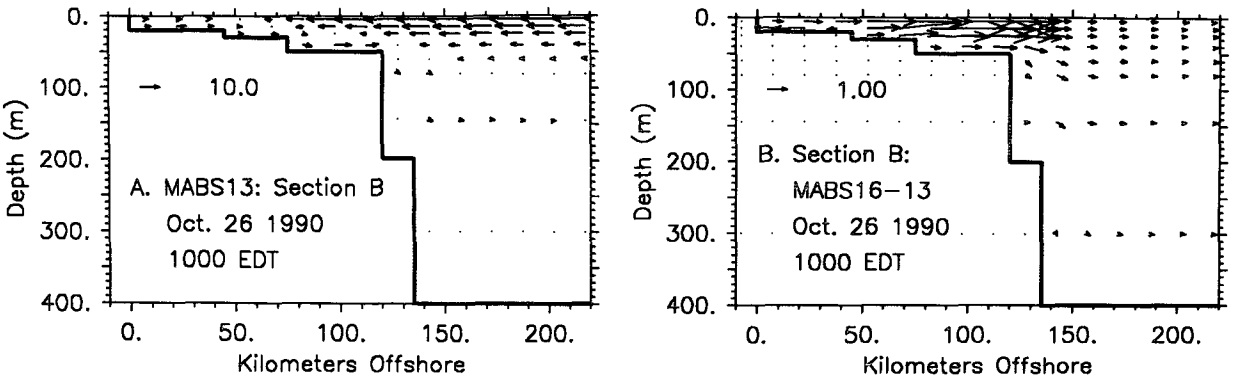

FIG. 5. The across-shelf flow field (cm s^{-1}) at section B at 1000 EDT 26 Oct. (a) Flow for run MABS13. (b) Cross-shelf currents from run MABS16 minus those from MABS13. Note the change in scales. Vertical exaggeration is 100.

oscillations with periods of 4–12 hours, as reported by Beardsley and Haidvogel (1981) and Blumberg and Kantha (1985), are also apparent in the coastal water-level signal.

5. Storm circulation with tides

Hodographs of the time history of surface currents along section B (Fig. 8a) trace a loop when no tides are present, with currents first directed landward then seaward. However, the combined storm and tidal flow (Fig. 8b) from hindcast MABS17 (see Table 1) presents a more cyclic and complex history. The combined storm flow is discussed in detail below with respect to sea surface height, surface and bottom currents, and cross-shelf flow patterns. It is convenient to focus on nine instances encompassing consecutive semidiurnal tidal periods that include the rise and fall of the storm surge and a change in wind direction. The analysis begins at low tide at 1800 EDT 25 October as indicated by the dashed vertical line in Fig. 7.

a. Sea surface height

Hindcast coastal water levels (Fig. 7) are similar in amplitude and phase to the observations. However, they are consistently low because of the location of the tide gauges at the coast whereas the model-calculated water levels are averages for 15 km × 15 km grid elements. The model also does not include the effects of coastal wave setup or reduced atmospheric pressure. Furthermore, because of the passage of a previous storm system (as seen in hindcast winds from the National Meteorological Center), the observed coastal water levels were elevated when the hindcast period began, whereas the model was initialized with only the tidal signal. The storm surge first developed at Duck Pier because of its proximity to the storm track and peaked during the flood tide just after midnight on 26 October. The storm-surge maxima in the northern MAB occurred progressively later within the tidal cycle because of a lag in coastal setup in conjunction with a tidal phase lead.

The increasing northerly winds during the evening of 25 October (see Fig. 2a) produced a significant storm surge within the southern MAB by low tide at 1800 EDT (Fig. 9a). During the following flood tide (Fig. 9b) the hindcast storm surge remained higher in the south although it was increasing within the central MAB. The following high tide arrived first in the north

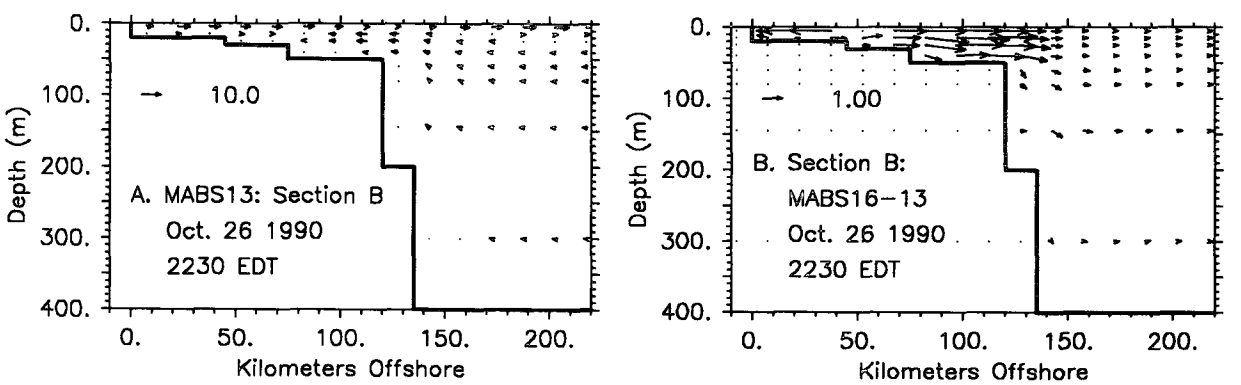

FIG. 6. The across-shelf flow field (cm s^{-1}) at section B at 2230 EDT 26 Oct. (a) Flow for run MABS13. (b) Cross-shelf currents from run MABS16 minus those from MABS13. Note the change in scales. Vertical exaggeration is 100.

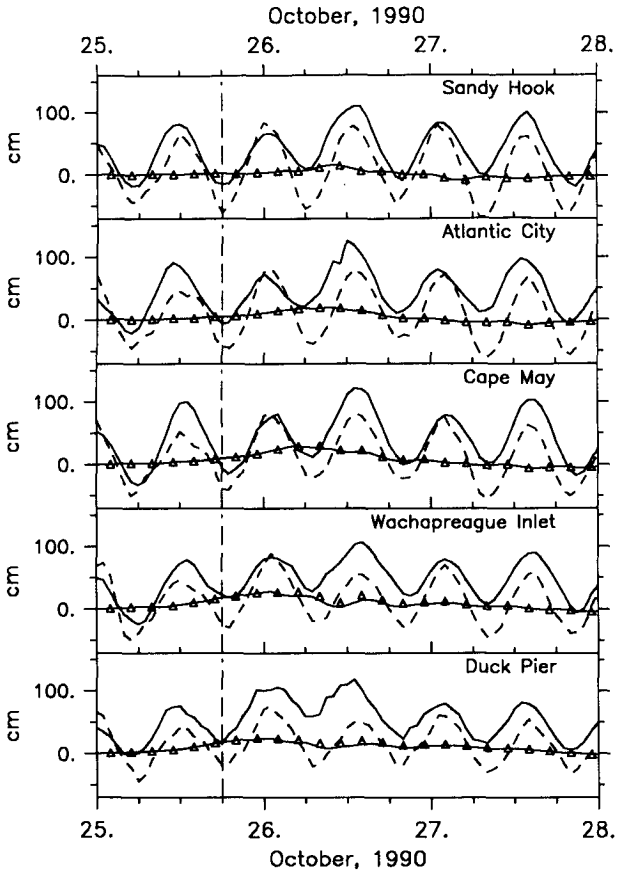

FIG. 7. Time series of coastal water levels. Observations from tide stations located in Fig. 1 are indicated by the solid line that contains tidal oscillations. The results for every 3 hours from the hindcast with $C_d = 0.00365$ (MABS14), and no tides are indicated by Δ. The solid line with no tidal oscillations indicates the results for MABS16, which uses the bottom boundary layer model to calculate C_d. The dash line represents the results from MABS17. The vertical dashed line indicates 1800 EDT 25 Oct.

(Fig. 9c) because of the slight phase difference within the MAB, at which time the storm setup peaked in the south. The hindcast coastal setup peaked at Cape May during the ebb tide (Fig. 7) and remained elevated at Duck Pier, while just beginning to rise at Sandy Hook. Thus sea surface heights were elevated within the central and southern MAB during ebb tide (Fig. 9d).

A second low tide occurred on the morning of 26 October (Fig. 9e), but coastal water levels were less coherent than earlier because of the transient responses discussed above (compare to Fig. 9a). The wind stresses had doubled from 12 h previously and had begun to rotate seaward over the southern MAB (see Fig. 2b), maintaining water levels near Chesapeake Bay. Coastal setup peaked in the north at mid-flood tide (Fig. 9f), but sea surface heights were flat elsewhere. Because of the decreasing storm surge in the south and the later development of coastal setup in the north, sea surface height was higher in the north at high tide (Fig. 9g), although there was a small peak at Chesapeake Bay. Coastal water levels at ebb tide (Fig. 9h) were uniform throughout the MAB except for a small peak at Cape May because of sustained alongshore winds over the central region. Sea surface heights in the model remained elevated in the south at low tide (Fig. 9i).

b. Surface flow

Low tide occurred at approximately 1800 EDT 25 October in hindcast MABS17. Surface flow was weak and parallel to isobaths (Fig. 10a) in the north and was stronger and increasingly seaward toward the south because of increasing coastal setup and tidal lag. Currents in the south decreased from 30 cm s^{-1} on the outer shelf to less than 20 cm s^{-1} near the coast. During the flood tide (Fig. 10b) currents were rotated landward at all water depths and increased to about 40 cm s^{-1} on the outer shelf in the south. A weak flow was present at the coast throughout the model domain. Figure 10c shows the surface flow at 0012 EDT 26 October when the hindcast tide was cresting in the north. Despite the landward flow resulting from the flood tide in the central and southern MAB, surface flow had a weaker landward component in the south because the storm setup opposed tidal flow. The southward flow near the coast strengthened in the vicinity of Chesapeake Bay. The southward wind stresses increased during ebb tide, and coastal setup stabilized in the south while continuing to rise in the north. The strong currents near the coast during the flood tide were no longer present at ebb tide (Fig. 10d), and currents were seaward everywhere with maximum speeds less than 50 cm s^{-1}.

The next low tide occurred at approximately 0624 EDT 26 October (Fig. 10e), and because of the high wind stresses and storm setup existing throughout the MAB, maximum hindcast surface currents increased to 50 cm s^{-1}. However, low tide came slightly later in the south, and therefore, flow was still offshore. The maximum storm surge occurred in the northern MAB during the flood tide, whereas storm setup was falling in the southern and central MAB (see Fig. 7). The

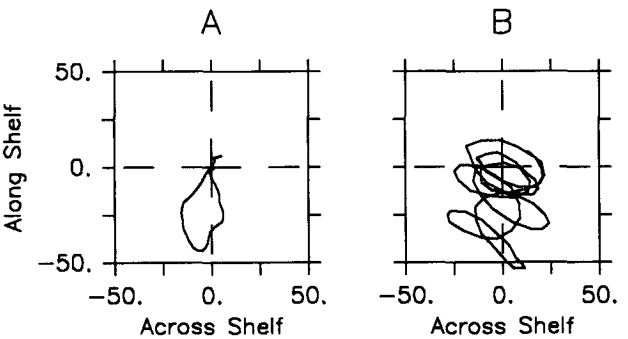

FIG. 8. Hodographs of time series of surface currents for (a) MABS16 and (b) MABS17 at section B.

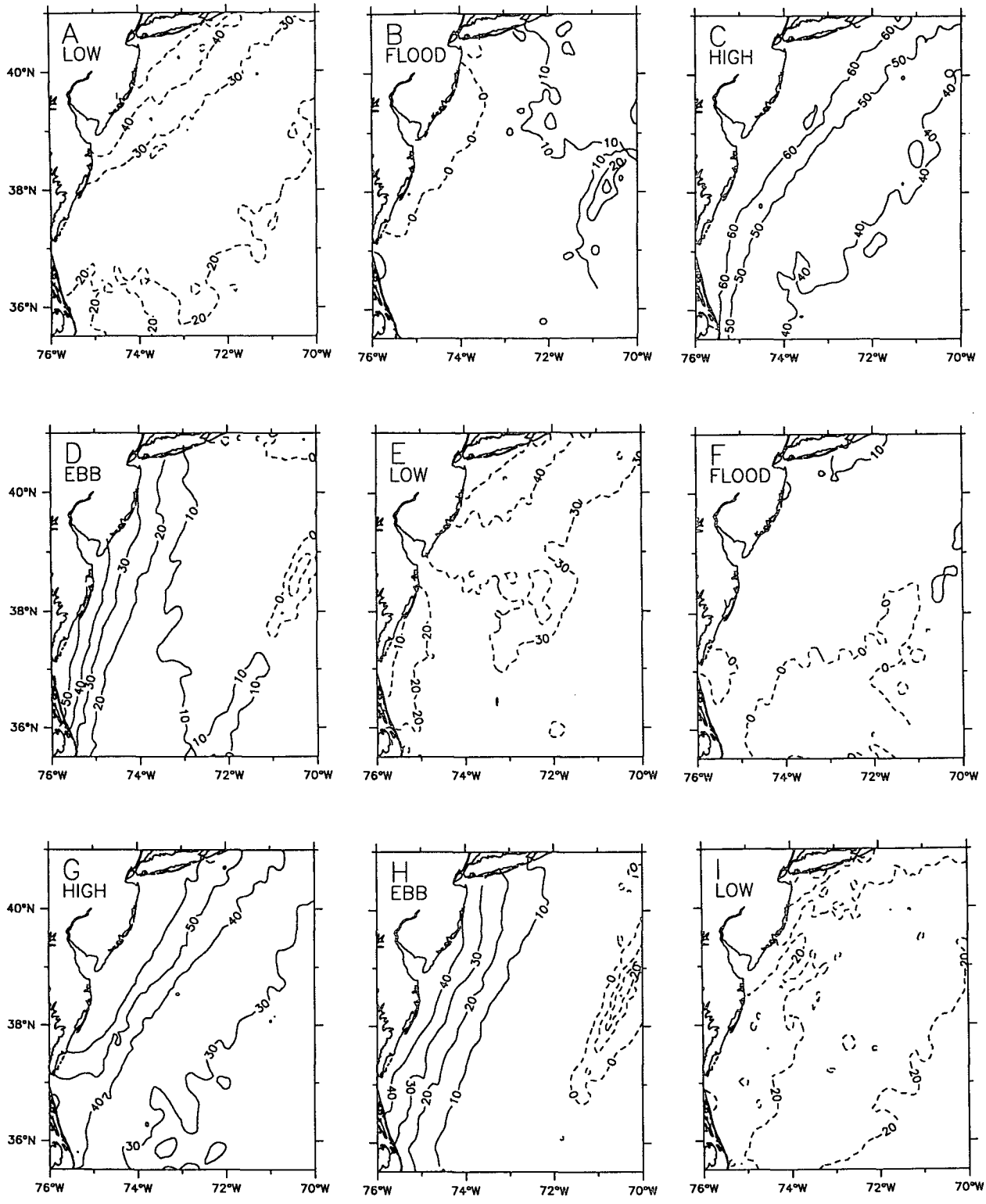

FIG. 9. Plots of sea surface height (cm) for hindcast MABS17 at successive phases of the tide: (a) low tide, 1800 EDT 25 Oct; (b) flood tide; (c) high tide, 0012 EDT 26 Oct; (d) ebb tide; (e) low tide, 0624 EDT; (f) flood tide; (g) high tide, 1236 EDT; (h) ebb tide; and (i) low tide, 1848 EDT. The contour interval is 10 cm. Positive values are indicated by solid lines and negative by dashed. Low, flood, high, and ebb tides, as indicated by coastal water levels at Sandy Hook, are indicated on the figures.

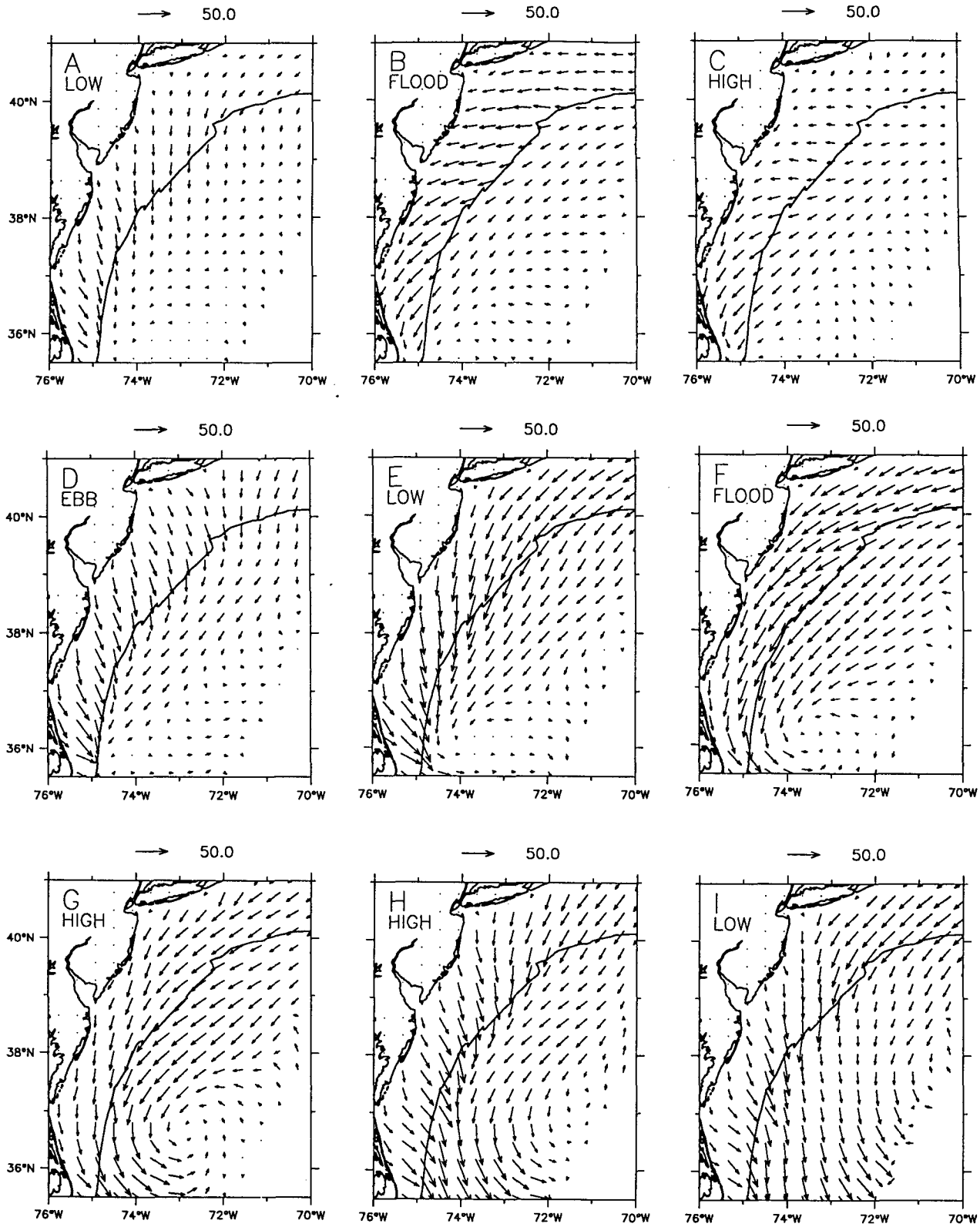

FIG. 10. Plots of surface currents (cm s^{-1}) for hindcast MABS17 at successive phases of the tide: (a) low tide, 1800 EDT 25 Oct; (b) flood tide; (c) high tide, 0012 EDT 26 Oct; (d) ebb tide; (e) low tide, 0624 EDT; (f) flood tide; (g) high tide, 1236 EDT; (h) ebb tide; and (i) low tide, 1848 EDT. The 200-m isobath is indicated by the solid offshore line. Low, flood, high, and ebb tides, as indicated by coastal water levels at Sandy Hook, are indicated on the figures.

additional pressure gradient, in combination with increased wind stresses, drove strong alongshelf flow everywhere (Fig. 10f) despite onshore tidal flow. The alongshelf coastal flow was stronger than previously as well. High tide coincided with the peak storm winds, which maintained strong surface flow throughout the region (Fig. 10g). The wind stress decreased, and the storm winds rotated offshore during ebb tide, and, although the hindcast currents (Fig. 10h) weakened somewhat in response, strong flow continued, driven by the falling storm surge throughout the MAB. Low tide came at approximately 1848 EDT as the storm winds were shifting to offshore, and surface flow (Fig. 10i) was strongly offshore in the central and southern MAB because of the lag in tides and sustained high coastal water levels in the south.

c. *Bottom flow*

Hindcast bottom flow in the northern MAB was very weak at 1800 EDT 25 October (Fig. 11a) when the tide was out. The largest currents of less than 20 cm s^{-1}, located near the 200-m isobath in the south, were directed almost directly offshore. The high angle between surface and bottom currents in the south (compare Figs. 10a and 11a) was possible because of persistent stratification that isolated the bottom flow from the wind stress. The effect of stratification was more apparent during the flood tide (Fig. 11b), with shoreward deflection of bottom currents by as much as 40° relative to the surface currents. The coastal flow at the surface was lacking at the bottom. Bottom currents at high tide (Fig. 11c) were negligible throughout the MAB. During the ebb tide (Fig. 11d) currents were offshore everywhere with peak magnitudes of about 30 cm s^{-1} in the south.

The low tide at 0624 EDT occurred first in the northern MAB (Fig. 11e) and bottom currents, while being very weak, were approximately parallel to isobaths. Toward the south, however, both magnitudes and offshore components increased and flow was nearly aligned with surface flow. Hindcast bottom circulation during the flood tide (Fig. 11f) was similar to that at the surface with maximum currents of less than 30 cm s^{-1}. This flow continued until high tide (Fig. 11g) but weakened slightly. A strong flow near the coast was present in the south at this time. By ebb tide bottom flow was offshore (Fig. 11h) with currents as high as 25 cm s^{-1}. This flow structure remained as currents weakened until, by low tide (Fig. 11i), bottom flow was similar to that before the storm everywhere.

d. *Cross-shelf flow patterns*

The previous discussion of the hindcast combined flow field during the storm revealed periodic variations in both the magnitudes and directions of currents on the shelf because of tidal flow. These periodic changes can be seen more clearly along the cross sections indicated in Fig. 1. The following discussion focuses on cross-shelf currents during flood and ebb tides that coincided with the storm peak when downwelling-favorable wind stresses were fairly uniform within the MAB.

Ekman surface drift and tidal currents at section A were superimposed during flood tide (Fig. 12a). The resulting hindcast flow was uniformly onshore throughout the water column, with maximum cross-shelf currents less than 10 cm s^{-1} at the bottom. Surface currents did not reverse direction with the ebbing tide (Fig. 12b), but the onshore component was reduced. Flow near the bottom did reverse and was offshore during the ebb tide. The wind stresses were parallel to the coast at section B during the flood tide. Consequently, predicted onshore surface flow (Fig. 12c) was strengthened by wind drift, whereas onshore bottom flow was reduced because of downwelling storm currents. Hindcast flow was uniformly offshore during the following ebb tide (Fig. 12d), with bottom currents resulting from combined tidal and downwelling flow. Hindcast currents at section C were uniformly offshore during the flood tide (Fig. 12e) because of offshore flow driven by the large storm surge in the south as well as coastal flow convergence. Offshore flow during the ebb tide (Fig. 12f) was strengthened because storm-surge ebb currents, downwelling bottom currents, and tidal currents were all in the same direction.

5. Discussion

Current measurements are not available for IOP-1. An alternative way of estimating hindcast error would be to use the hindcast and observed coastal water levels, but such an analysis would not reflect model performance since the differences seen in Fig. 7 can be attributed to identified sources that were neglected in the model. Before these analyses can be performed, the model grid near the coast must be improved and current measurements need to be made during storms. Nevertheless, several datasets collected within the MAB during storms can be used to qualitatively evaluate the hindcast results. The discussion will then focus on the implications of the hindcast results for storm flows and sedimentation on the MAB continental shelf.

a. *Observations from the Middle Atlantic Bight*

Storm currents within the MAB can vary considerably depending on stratification. Swift et al. (1986) discuss currents (averaged over a storm period) during winter and summer storms. Currents during a storm in February 1974 were primarily alongshelf, with magnitudes of approximately 40 cm s^{-1} near the surface in water depths of 35 m. Cross-shelf flow was unusually well developed during an August storm in the same year. These cases represent extremes of stratification, however, and October is an intermediate period when

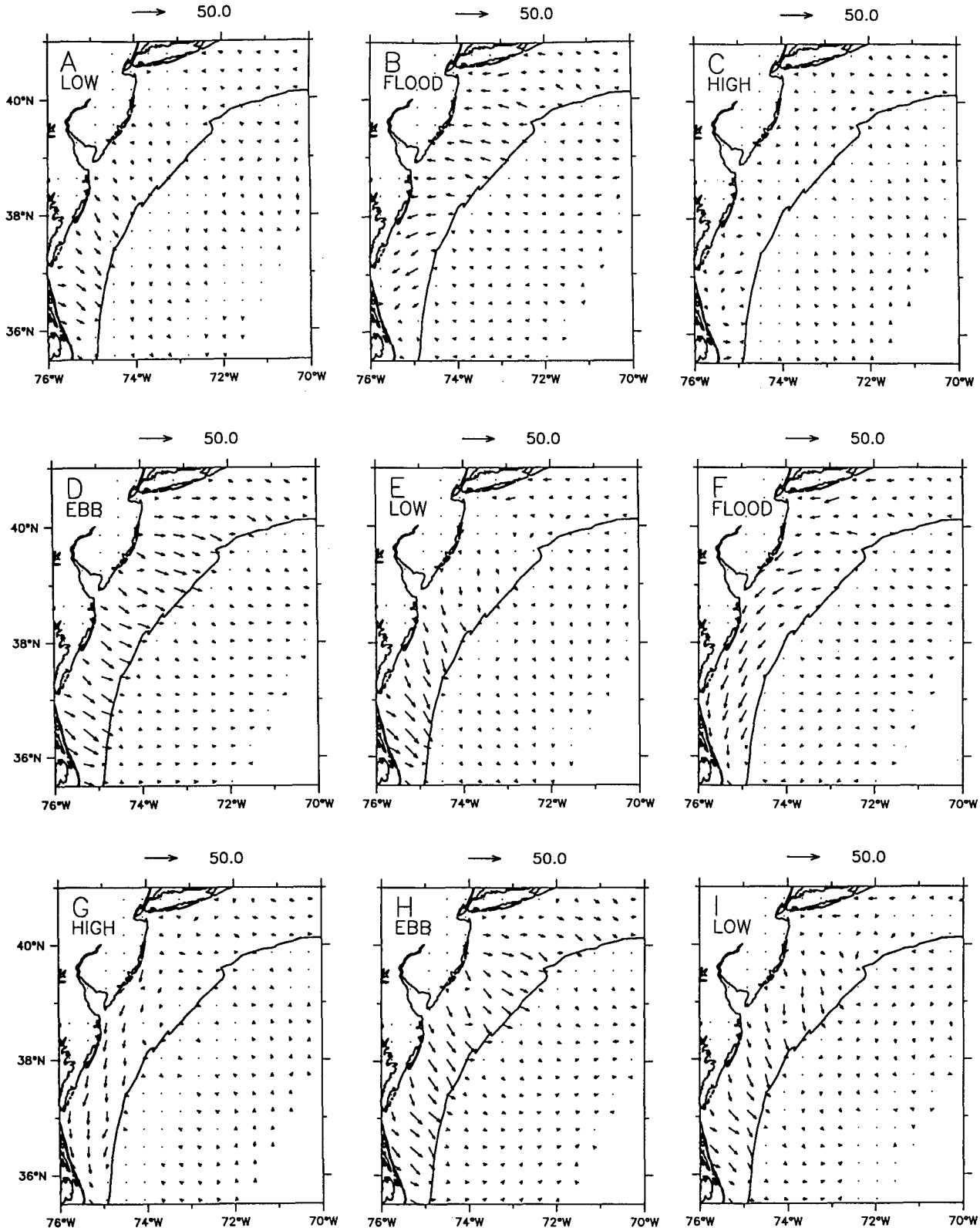

FIG. 11. Plots of bottom currents (cm s^{-1}) for hindcast MABS17 at successive phases of the tide: (a) low tide, 1800 EDT 25 Oct; (b) flood tide; (c) high tide, 0012 EDT 26 Oct; (d) ebb tide; (e) low tide, 0624 EDT; (f) flood tide; (g) high tide, 1236 EDT; (h) ebb tide; and (i) low tide, 1848 EDT. Low, flood, high, and ebb tides, as indicated by coastal water levels at Sandy Hook, are indicated on the figures.

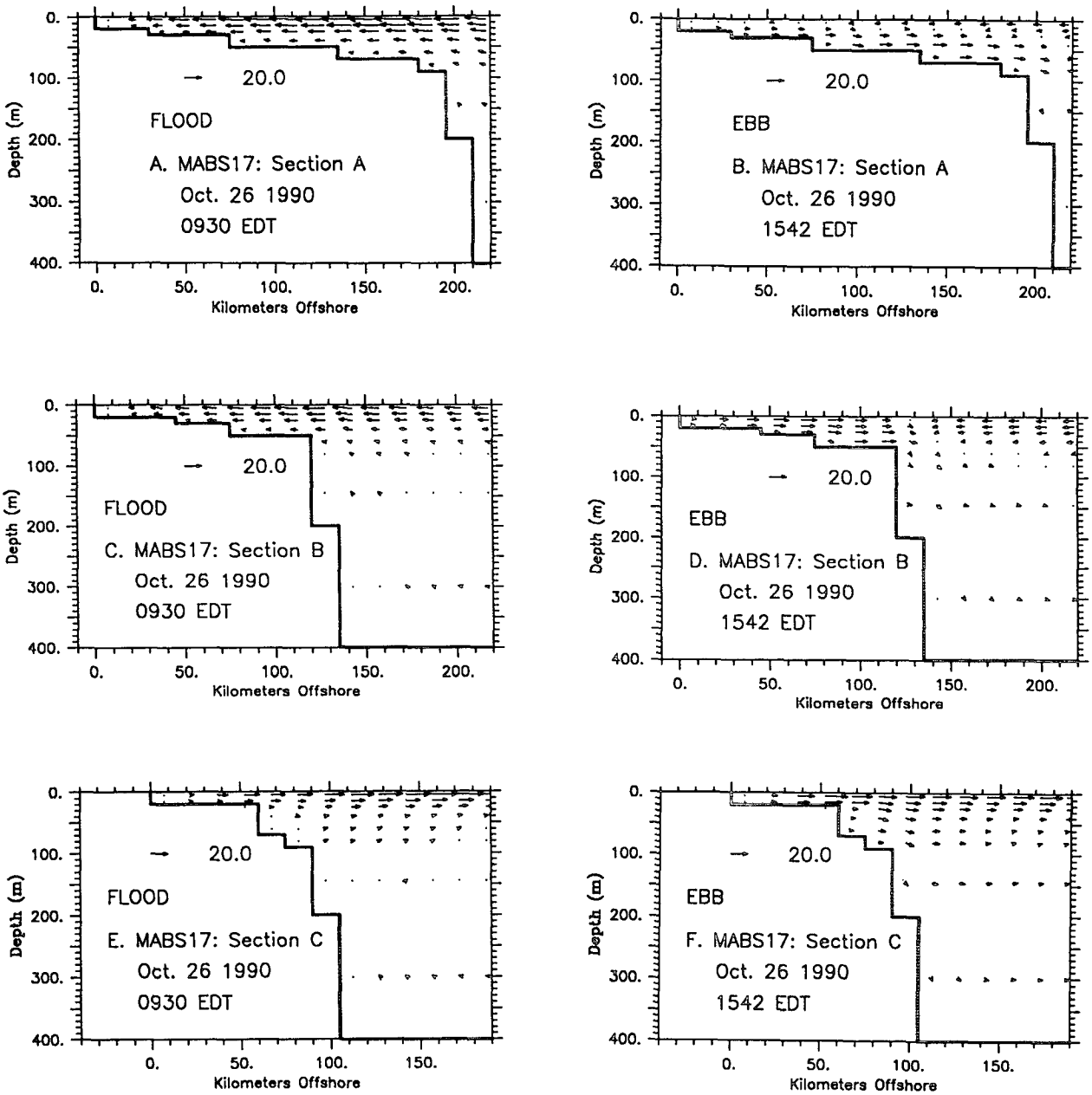

FIG. 12. Cross-shelf flow field (cm s^{-1}) from hindcast MABS17 during the main storm period along (a) cross section A at flood tide and (b) ebb tide, (c) cross section B at flood tide and (d) ebb tide, and (e) section C at flood tide and (f) ebb tide. Vertical exaggeration (V.E.) is 100. The tide stage, as indicated by coastal water levels at Sandy Hook, is indicated on the figures.

winter mixing is incomplete. The storm flow regime during the SWADE storm should be intermediate between these examples. The surface flow at section B attained speeds of about 50 cm s^{-1} (see Fig. 4) and was primarily alongshelf. This is supported by the weak cross-shelf flow in Fig. 5a. Variation in cross-shelf flow with depth, as seen in the hindcast results, is suggested by the cross-shelf component of currents during the August 1974 storm. This two-layer flow regime can be seen in Fig. 5a.

Scott and Csanady (1976) measured currents at a water depth of 32.5 m on the Long Island shelf during a storm in late September when stratification was stronger than that used in the SWADE hindcasts. The alongshelf (downwelling favorable) wind stress was approximately 2.5 dyn cm^{-2} to the west. The observations were averaged over a diurnal tidal period to remove the primary source of tidal variability. Surface currents were in the wind direction and did not vary significantly from 40 cm s^{-1} between 3.5 and 16 m

below MSL. Measured currents at the bed were rotated 20° offshore. Typical hindcast currents at a similar water depth for the SWADE storm upper model level (5 m below MSL) were in the wind direction with velocities of about 40 cm s^{-1}, but magnitudes decreased downward while currents rotated offshore by approximately 20° at the bed. Both observed and hindcast currents were approximately 20 cm s^{-1} at the bottom. The difference between the observed and hindcast current structure at middepth can be attributed to differences in stratification for the two storms. Profiles of σ_T from the Long Island shoreface prior to the September storm indicate a pycnocline near the bottom, whereas the pycnocline near the surface in Fig. 3 was also present in shallow water in the SWADE hindcast. Thus, middepth flow was less directly forced by the wind stress in the SWADE hindcast.

Peak alongshelf bottom currents during storms exceed 30 cm s^{-1} at depths of 60 m within the MAB (Butman et al. 1979; Lyne et al. 1990a). The hindcast bottom currents on the middle shelf (Fig. 11) were this strong during the storm peak and varied from alongshelf during flood and slack tides to offshore during ebb tides. However, the model domain and boundary conditions used in the present study resulted in weaker flow in the north because of the reduced alongshelf pressure gradient.

Observations summarized by Glenn and Ebbesmeyer (1994) suggest that the direct influence of the Gulf Stream on the shelf waters of the MAB during storms is minor. Gulf Stream water has been observed 13%–27% of the time on the upper slope and 3%–9% of the time on the shelf between 36° and 38°N over an 11-year period (Churchill and Cornillon 1990). Gulf Stream water has also been identified in water depths of 10–30 m on the shelf immediately north of Cape Hatteras (Gawarkiewicz et al. 1992), but these intrusions are along the base of the thermocline and therefore will have little effect on sediment transport near the bed.

b. *Combined storm and tidal circulation*

Storms of a few days duration can generate event flows (Seilacher 1982) that last long enough for astronomical tides to contribute significantly to flow on continental shelves where tidal currents are of order 10 cm s^{-1}. Figure 8 shows the combined flow resulting from storm and tidal currents during the SWADE storm, with the oscillatory motion of the tides superimposed on a net alongshelf drift to the southwest. The previous discussion, however, has shown that the resultant flow is not simply the sum of the two components because of the evolving balance between pressure gradients and wind stresses. This nonlinear interaction of tidal and wind-driven currents was also discussed by Davies and Lawrence (1993). Net transport can also result from asymmetries in tidal flow alone in bays and estuaries where bathymetry is highly variable (Blumberg et al. 1993).

The effects of combined wave–current bottom stresses generally followed the patterns summarized by Keen and Glenn (1994), with currents reduced on the inner shelf and rotated offshore near the bed on the outer shelf. The simple pattern associated with uniform winds and simple geometry did not fully develop in the SWADE hindcasts, however, because of changing wind stresses and local geometric variability within the MAB.

Stratification during the SWADE storm produced somewhat different results than those observed by Forristall et al. (1977) and those modeled by Spaulding and Isaji (1987) and by Keen and Slingerland (1993a,b) for well-mixed shelf waters during tropical cyclones. The weak October stratification used in the hindcasts persisted during the storm and maintained two-layer flow and downwelling on the outer shelf. Stratification allowed the surface flow to remain primarily wind forced, while the storm surge and astronomical tides drove bottom currents more effectively. Such flow structure is generally lacking in the well-mixed water column during the tropical cyclones studied by the above authors.

c. *Implications for storm sedimentation*

The effect of the combined wave and current flow on sediment entrainment can be evaluated using time series of the average friction velocity u_c^* (Grant and Madsen 1979) at the three cross sections discussed

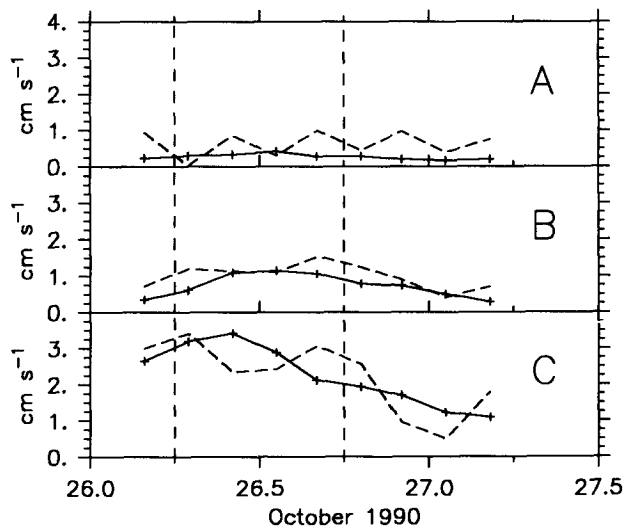

FIG. 13. Time series of u_c^* (cm s^{-1}) at successive phases of the tide for (a) a 30-m station on section A, (b) a 20-m location along section B, and (c) a station at a depth of 20 m on section C. The results for hindcast MABS16 (without tides) are shown by a solid line and those for MABS17 (with tides) by a dashed line. The locations are at midshelf positions. The vertical lines indicate approximate high tides.

above (see Fig. 1 for locations). The storm's influence was weakest in the northern MAB; u_c^* at section A (Fig. 13a) alternates between maximum values during flood and ebb tides and minimum values during slack water. High tides are indicated by vertical dashed lines in Fig. 13. The storm peak within the central MAB (Fig. 13b) is indicated by the largest u_c^* in the tideless hindcast (solid line). When tides were present, the maximum bottom stresses occurred later because of the combined offshore flow of the ebbing storm and astronomical tides. Very little fluctuation occurred after the peak, as offshore rotation of the storm winds and ebbing of the storm surge maintained relatively high flows during low tide and countered the flood tide late on 26 October. The storm's influence on sedimentation was greatest in the southern MAB as indicated in time series of u_c^* (Fig. 13c). When tides were neglected, the maximum bottom stress occurred at approximately day 26.4. When tides were present, the peak bottom stress was shifted approximately 3 hours ahead to the preceding low tide. A second peak occurred during ebb tide at about day 26.7 as in section B. The first peak was the result of strong storm flow during a low tide, whereas the second peak was caused by a combination of a weaker storm flow and ebb tide currents.

Sediment entrainment is a function of the instantaneous shear stress at the bed. The wave–current shear velocities above the wave boundary layer (Fig. 13) can be used to infer the timing of sediment entrainment during the SWADE storm. Entrainment would have been high first during the peak storm currents at low tide along sections B and C and later during the ebb tide. Maximum entrainment would have coincided with the storm peak in the south, whereas the weaker storm currents in the central MAB would have allowed the greatest entrainment during the ebb tide.

The large values of u_c^* at approximately 0600 EDT 26 October coincide with strong offshore bottom flow within the central and southern MAB (Fig. 11e). Sediment would have been transported from the inner to outer shelf at this time, but because of the decrease in shear stresses during the following flood tide, transport distances would have been limited. The second interval of large shear stresses occurred during ebb tide (Fig. 11h) when bottom currents were almost directly offshore. This second pulse of sediment transport reinforced the first and would have moved entrained sediment farther offshore. However, since shear stresses in the south remained elevated for the entire storm period, there would have been intermittent transport to the southwest as well.

6. Conclusions

This paper has focused on the effects of combined wave–current bottom shear stresses and tidal flow on circulation during an extratropical cyclone as a step toward understanding storm sedimentation patterns within the MAB. The hindcast storm flow within the central part of the Middle Atlantic Bight was similar to that from an idealized shelf with steady winds (Keen and Glenn 1994) but was more complex because of a change in winds from downwelling favorable to offshore during the storm's passage. Flow within the southern part of the MAB, where the coast is oriented more to the southeast, was characterized by consistent offshore near-bottom flow because the winds were downwelling favorable during most of the storm. Storm currents were consistently stronger in the south because of coastal geometry and the proximity of the storm track.

Increasing bottom roughness and friction did not produce a simple response because of variations in storm winds and local topographic effects. Currents in shallow water were reduced by combined bottom friction, and currents on the outer shelf were rotated slightly offshore relative to the constant drag coefficient hindcasts.

A more important effect was found with the inclusion of tidal forcing in the hindcasts. Tidal currents were of similar magnitudes as the storm currents, so the combined flow varied periodically with the flood and ebb of the tide. The influence of the tides was more pronounced at the bottom than at the surface. This result has important implications for sedimentation during extratropical cyclones. Combined wave–current bottom shear stresses are influenced by the combined tidal and storm steady currents, as well as the wave parameters at the bottom, and peak sediment entrainment and transport are tied to the tidal cycle. Although hindcast peak storm currents approximately coincided with low tide over much of the MAB during the storm, maximum sedimentation rates occurred at different times within the region. A quantitative analysis of hindcast sedimentation during the SWADE storm is discussed by Keen et al. (1994).

Acknowledgments. This work was completed while the first author was a postdoctoral fellow at the Institute of Marine and Coastal Sciences. The second author was partially supported by funds from the NOAA/NURP New York Bight Center. We wish to thank Vincent Cardone and Hans Graber for supplying the hindcast wind and wave fields used in this work, as well as William Gemmil and Robert Jensen for making the NMC hindcast winds available. Some hindcasts were run at the Cornell National Supercomputer Facility, a resource of the Cornell Theory Center, which receives major funding from the National Science Foundation and the IBM Corporation, with additional support from New York state and members of its Corporate Research Institute. We also wish to thank the anonymous reviewers whose comments helped to significantly improve the manuscript.

REFERENCES

Beardsley, R. C., and D. B. Haidvogel, 1981: Model studies on the wind-driven transient circulation in the Middle Atlantic Bight.

Part I: Adiabatic boundary conditions. *J. Phys. Oceanogr.*, **11**, 355–375.

Blumberg, A. L., and L. H. Kantha, 1985: Open boundary conditions for circulation models: *J. Hyd. Eng.*, **111**, 237–255.

——, R. P. Signell, and H. J. Lenter, 1993: Modelling transport processes in the coastal ocean. *J. Mar. Env. Eng.*, **1**, 31–52.

Bowman, M. J., 1977: Hydrographic properties. MESA New York Bight Project. New York Sea Grant Institute, 152 pp.

Butman, B., M. Noble, and D. W. Folger, 1979: Long-term observations of bottom currents and bottom sediment movement on the Mid-Atlantic continental shelf. *J. Geophys. Res.*, **84**, 1187–1205.

Caruso, M. J., H. C. Graber, R. E. Jensen, and M. A. Donelan, 1993: Observations and modelling of winds and waves during the surface wave dynamics experiment. Tech. Rep. CERC-93-6. U.S. Army Corps of Engineers, 195 pp.

Churchill, J. H., and P. C. Cornillon, 1990: Gulf Stream water on the shelf and upper slope north of Cape Hatteras. *Cont. Shelf Res.*, **11**, 409–431.

Davies, A. M., and J. Lawrence, 1993: A wind-driven high-resolution model of the eastern Irish Sea, including wave–current interaction. *J. Phys. Oceanogr.*

Forristall, G. Z., R. C. Hamilton, and V. J. Cardone, 1977: Continental shelf currents in Tropical Storm Delia: Observations and theory. *J. Phys. Oceanogr.*, **7**, 532–546.

Gadd, P. E., J. W. Lavelle, and D. J. P. Swift, 1978: Estimates of sand transport on the New York shelf using near-bottom current-meter observations. *J. Sed. Petrol.*, **48**, 239–252.

Gawarkiewicz, G., T. M. Church, G. W. Luther III, T. G. Ferdelman, and M. Caruso, 1992: Large-scale penetration of Gulf Stream water onto the continental shelf north of Cape Hatteras. *Geophys. Res. Lett.*, **19**, 373–376.

Glenn, S. M., and W. D. Grant, 1987: A suspended sediment stratification correction for combined wave and current flows. *J. Geophys. Res.*, **92**, 8244–8264.

——, and C. E. Ebbesmeyer, 1994: Observations of Gulf Stream frontal eddies in the vicinity of Cape Hatteras. *J. Geophys. Res.*, **99**, 5047–5055.

Grant, W. D., and O. S. Madsen, 1979: Combined wave and current interaction with a rough bottom. *J. Geophys. Res.*, **84**, 1797–1808.

——, and ——, 1982: Moveable bed roughness in unsteady oscillatory flow. *J. Geophys. Res.*, **87**, 469–481.

Johnson, H. K., and H. J. Vested, 1992: Effects of water waves on wind shear stress for current modeling. *J. Atmos. Oceanic Technol.*, **9**, 850–861.

Keen, T. R., and R. L. Slingerland, 1993a: A numerical study of sediment transport and event bed genesis during Tropical Storm Delia. *J. Geophys. Res.*, **98**, 4775–4791.

——, and ——, 1993b: Four storm-event beds and the tropical cyclones that produced them: A numerical hindcast. *J. Sed. Petrol.*, **63**, 218–232.

——, and S. M. Glenn, 1994: A coupled hydrodynamic–bottom boundary layer model of Ekman flow on stratified continental shelves. *J. Phys. Oceanogr.*, 1732–1749.

——, ——, and R. L. Slingerland, 1994: *Proc., 3rd Int. Conf. Estuarine and Coastal Modeling.* III. A.S.C.E., 279–293.

Leendertse, J. J., and S. K. Liu, 1977: A three-dimensional model for estuaries and coastal seas, Vol. IV. *Turbulent Energy Computation.* Report R-2187-OWRT, Rand Corporation, 97 pp.

Liu, S. K., and J. J. Leendertse, 1978: *Hydrodynamics of Estuaries and Fjords.* Elsevier, 387–405.

Lyne, V. D., B. Butman, and W. D. Grant, 1990a: Sediment movement along the U.S. east coast continental shelf—I. Estimates of bottom stress using the Grant-Madsen model and near-bottom wave and current measurements. *Contin. Shelf Res.*, **10**, 397–428.

——, ——, and ——, 1990b: Sediment movement along the U.S. east coast continental shelf—II. Modelling suspended sediment concentration and transport rate during storms. *Contin. Shelf Res.*, **10**, 429–460.

Neumann, G., and W. J. Pierson, Jr., 1966: *Principles of Physical Oceanography.* Prentice-Hall, 545 pp.

Scott, J. T., and G. T. Csanady, 1976: Nearshore currents off Long Island. *J. Geophys. Res.*, **81**, 5401–5409.

Schwiderski, E. W., 1979: Global Ocean tides. Part II: The semidiurnal principal lunar tide (M_2). Atlas of Tidal Charts and Maps, Report NSWC Tr 79-414, Naval Surface Weapons Center, 115 pp.

Seilacher, A., 1982: *Cyclic and Event Stratification.* Springer-Verlag, 161–174.

Spaulding, M. L., and T. Isaji, 1987: *Three Dimensional Models of Marine and Estuarine Dynamics.* Elsevier, 405–426.

Swift, D. J. P., and J. A. Thorne, 1991: Shelf sand and sandstone bodies: Geometry, facies, and sequence stratigraphy. *Spec. Pub., Int. Assoc. Sediment.*, **14**, 3–32.

——, J. P. Han, and C. E. Vincent, 1986: *Shelf Sands and Sandstone Reservoirs.* Canadian Society of Petroleum Geologists, 99–119.

Trowbridge, J. H., and S. J. Lentz, 1991: Asymmetric behavior of an oceanic boundary layer above a sloping bottom. *J. Phys. Oceanogr.*, **21**, 1171–1185.

Vincent, C. E., D. J. P. Swift, and B. Hillard, 1981: *Sedimentary Dynamics on Continental Shelves.* Elsevier, 369–398.

Weller, R. A., M. A. Donelan, M. G. Briscoe, and N. E. Huang, 1991: Riding the crest: A tale of two wave experiments. *Bull. Amer. Meteor. Soc.*, **72**, 163–183.